NHS Breast Screening Programme Equipment Report

Technical Evaluation of Siemens Revelation digital mammography system in 2D mode

March 2019

About Public Health England

Public Health England exists to protect and improve the nation's health and wellbeing, and reduce health inequalities. We do this through world-leading science, knowledge and intelligence, advocacy, partnerships and the delivery of specialist public health services. We are an executive agency of the Department of Health and Social Care, and a distinct delivery organisation with operational autonomy. We provide government, local government, the NHS, Parliament, industry and the public with evidence-based professional, scientific and delivery expertise and support.

Public Health England, Wellington House, 133-155 Waterloo Road, London SE1 8UG
Tel: 020 7654 8000   www.gov.uk/phe
Twitter: @PHE_uk   Facebook: www.facebook.com/PublicHealthEngland

About PHE screening

Screening identifies apparently healthy people who may be at increased risk of a disease or condition, enabling earlier treatment or informed decisions. National population screening programmes are implemented in the NHS on the advice of the UK National Screening Committee (UK NSC), which makes independent, evidence-based recommendations to ministers in the 4 UK countries. PHE advises the government and the NHS so England has safe, high quality screening programmes that reflect the best available evidence and the UK NSC recommendations. PHE also develops standards and provides specific services that help the local NHS implement and run screening services consistently across the country.

www.gov.uk/phe/screening Twitter: @PHE_Screening Blog: phescreening.blog.gov.uk
For queries relating to this document, please contact: phe.screeninghelpdesk@nhs.net
Prepared by: N Tyler, A Mackenzie
The image on page 7 is courtesy of Siemens.
© Crown copyright 2018
You may re-use this information (excluding logos) free of charge in any format or medium, under the terms of the Open Government Licence v3.0. To view this licence, visit OGL or email psi@nationalarchives.gsi.gov.uk. Where we have identified any third party copyright information you will need to obtain permission from the copyright holders concerned.

Published XXXXXXXX
PHE publications gateway number: 201XXXX

Corporate member of
Plain English Campaign
Committed to clearer
communication
339

Contents

Executive summary

The purpose of the evaluation was to determine whether the Siemens Revelation operating in 2D mode, meets the main standards in the NHS Breast Screening Programme (NHSBSP) and European protocols, and to provide performance data for comparison against other systems.

The mean glandular dose (MGD) was found to be well below the remedial level for all automatic exposure control (AEC) dose modes. For a 53mm equivalent standard breast, the MGD was 0.86mGy, compared with the remedial level of 2.5mGy. The image quality, measured by threshold gold thickness using the CDMAM test object, is at the achievable level.

The Siemens Revelation meets the requirements of the NHSBSP standards for digital mammography systems operating in 2D mode.

1. Introduction

1.1 Testing procedures and performance standards for digital mammography

This report is one of a series evaluating commercially available direct digital radiography (DR) systems for mammography on behalf of the NHS Breast Screening Programme (NHSBSP). The testing methods and standards applied are mainly derived from NHSBSP Equipment Report 0604[1] which is referred to in this document as 'the NHSBSP protocol'. The standards for image quality and dose are the same as those provided in the European protocol,[2,3] but the latter has been followed where it provides a more detailed standard, for example, for the automatic exposure control (AEC) system.

Some additional tests were carried out according to the UK recommendations for testing mammography X-ray equipment as described in IPEM Report 89.[4]

1.2 Objectives

The aims of the evaluation were:

- to determine whether the Siemens Revelation digital mammography system, operating in 2D mode, meets the main standards in the NHSBSP and European protocols

- to provide performance data for comparison against other systems.

2. Methods

2.1 System tested

The tests were conducted at the Siemens factory in Forchheim, Germany on a Siemens Revelation system as described in Table 1. The Revelation is shown in Figure 1.

Table 1. System description

Manufacturer	Siemens Healthineers
Model	Revelation
System serial number	114
Target material	Tungsten (W)
Added filtration	50µm Rhodium (Rh)
Detector type	Amorphous selenium
Detector serial number	LV2-00007
Pixel size	85µm
Detector size	304.64mm x 239.36mm
Pixel array	2800 x 3518
Typical image sizes	14MB (20.1 mm x 26.9 mm field size)
	19MB (23.8 mm x 29.9 mm field size)
Pixel value offset	50
Source to detector distance	656mm (for broad and fine focus)
Source to table distance	636mm (for broad focus)
	469mm (for fine focus – Mag 1.5)
	397mm (for fine focus – Mag 1.8)
Pre-exposure mAs	5
Automatic exposure control (AEC) modes	OPDOSE, segmentation on or off, five dose levels: normal and ±10 or 20% and PRIME
Software version	VC10B\VD10B SL65P66 syngo VI10A
	SL46P60 (VZ10A)

The system tested was equipped with the PRIME (Progressive Reconstruction Intelligently Minimising Exposure) option, which may be used for breast thicknesses up to 70mm. Instead of the system using a grid, the software identifies structures in the breast that cause scatter, and subtracts the estimated scatter signal. The system is able to select a lower mAs when PRIME is in operation, as the X-rays are not absorbed by a grid. The dose saving depends on breast thickness but is typically 20% but may reduce image quality.

PRIME may be selected or deselected at the acquisition workstation. The AEC system has five dose settings: low, medium low, normal, medium high and high. These allow selection of dose levels 10% or 20% above or below normal dose.

The AEC is a "smart" system which identifies a denser region in the breast, a process known as segmentation. The system uses this denser region to select the appropriate exposure factors. If the tube is angled for an oblique view, a triangular region at the chest wall, corresponding to the expected position of pectoral muscle, is excluded from the search for a dense area.

Figure 1. The Siemens Revelation system

2.2 Output and HVL

The output and half-value-layer (HVL) were measured as described in the NHSBSP protocol, at intervals of 3kV.

2.3   Detector response

The detector response was measured as described in the NHSBSP protocol, except that 2mm aluminium was used at the tubehead, instead of PMMA. The grid was removed and an ion chamber was positioned above the breast support, 40mm from the chest wall edge (CWE). The incident air kerma was measured for a range of manually set mAs values at 29kV W/Rh anode/filter combination. The readings were corrected to the surface of the detector using the inverse square law. No correction was made for attenuation by the detector cover. A 10mm x 10mm region of interest (ROI) was positioned on the midline, 40mm from the CWE of each image. The average pixel value and the standard deviation of pixel values within the ROI were measured. The relationship between average pixel values and the incident air kerma to the detector was determined.

2.4   Dose measurement

Doses were measured using the X-ray set's various AEC modes to expose different thicknesses of PMMA. Each PMMA block had an area of 180mm x 240mm. Spacers were used to adjust the paddle height to be equal to the equivalent breast thickness, as shown in Table 3. The exposure factors were noted and mean glandular doses (MGDs) were calculated for breasts of equivalent thicknesses.

An aluminium square, 10mm x 10mm and 0.2mm thick, was used with the PMMA during these exposures, so that the images produced could be used for the calculation of the contrast-to-noise ratio (CNR), described in Section 2.5. The aluminium square was placed between two 10mm thick slabs of 180mm x 240mm PMMA, on the midline, with its centre 60mm from the CWE. Additional layers of PMMA were placed on top to vary the total thickness.

2.5   Contrast-to-noise ratio

Unprocessed images acquired during the dose measurement were analysed to obtain the CNRs. Thirty six small square ROIs (approximately 2.5mm x 2.5mm) were used to determine the average signal and the standard deviation in the signal within the image of the aluminium square (4 ROIs) and the surrounding background (32 ROIs), as shown in Figure 2. Small ROIs are used to minimise distortions due to the heel effect and other causes of non-uniformity.[5] The CNR was calculated for each image, as defined in the NHSBSP and European Protocols.
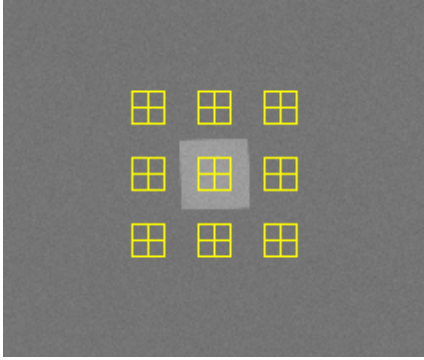
Figure 2. Location and size of ROI used to determine the CNR

To apply the standards in the European protocol, it is necessary to relate the image quality measured using the CDMAM (Section 2.8) for an equivalent breast thickness of 60mm, to that for other breast thicknesses. The European protocol[2] gives the relationship between threshold contrast and CNR measurements, enabling the calculation of a target CNR value for a particular level of image quality. This can be compared to CNR measurements made at other breast thicknesses. Contrast for a particular gold thickness is calculated using Equation 1, and target CNR is calculated using Equation 2.

$$Contrast = 1 - e^{-\mu t} \tag{1}$$

where μ is the effective attenuation coefficient for gold, and t is the gold thickness.

$$CNR_{target} = \frac{CNR_{measured} \times TC_{measured}}{TC_{target}} \tag{2}$$

where $CNR_{measured}$ is the CNR for a 60mm equivalent breast, $TC_{measured}$ is the threshold contrast calculated using the threshold gold thickness for a 0.1mm diameter detail, (measured using the CDMAM at the same dose as used for $CNR_{measured}$), and TC_{target} is the calculated threshold contrast corresponding to the threshold gold thickness required to meet either the minimum acceptable or achievable level of image quality as defined in the NHSBSP protocol.

The threshold gold thickness for the 0.1mm diameter detail is used here because it is generally regarded as the most critical of the detail diameters for which performance standards are set.

The effective attenuation coefficient for gold used in Equation 1 depends on the beam quality used for the exposure, and the value used is in Table 2. This value was calculated with 3mm PMMA representing the compression paddle, using spectra from Boone et al.[6] and attenuation coefficients for materials in the test objects (aluminium, gold, PMMA) from Berger et al.[7]

The European protocol also defines a limiting value for CNR, which is calculated as a percentage of the threshold contrast for minimum acceptable image quality for each thickness. This limiting value varies with thickness, as shown in Table 3.

Table 2. Effective attenuation coefficients for gold contrast details in the CDMAM

kV	Target/ filter	Effective attenuation coefficient (μm^{-1})
30	W/Rh	0.1247

Table 3. Limiting values for relative CNR

Thickness of PMMA (mm)	Equivalent breast thickness (mm)	Limiting values for relative CNR (%) in European protocol
20	21	> 115
30	32	> 110
40	45	> 105
45	53	> 103
50	60	> 100
60	75	> 95
70	90	> 90

The target CNR values for minimum acceptable and achievable levels of image quality and European limiting values for CNR were calculated. These were compared with the measured CNR results for all breast thicknesses.

2.6 AEC performance for local dense areas

This test is described in the supplement to the fourth edition of the European protocol.[3] To simulate local dense areas, images of a 30mm thick block of PMMA of size 180mm x 240mm, were acquired under AEC. Extra pieces of PMMA between 2 and 20mm thick and of size 20mm x 40mm were added to provide extra attenuation. The compression plate remained in position at a height of 40mm, as shown in Figure 3. The simulated dense area was positioned 50mm from the CWE of the breast support table.

In the simulated local dense area the mean pixel value and standard deviation for a 10mm x 10mm ROI were measured and the signal-to-noise ratios (SNRs) were calculated.
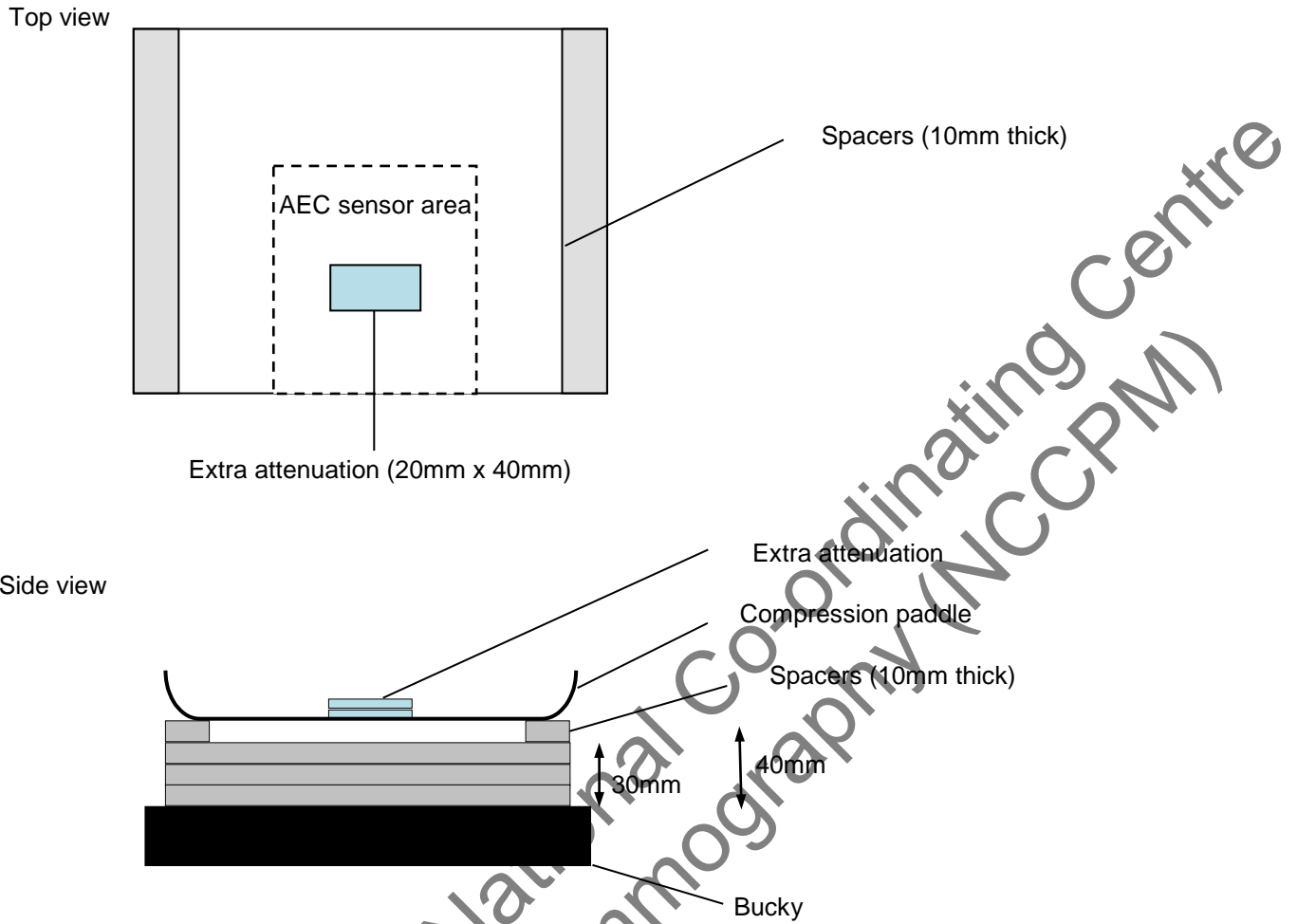
Top view

Side view

Figure 3. Setup to measure AEC performance for local dense areas

2.7 Noise analysis

The images acquired in the measurements of detector response, using 29kV W/Rh, were used to analyse the image noise. Small ROIs with an area of approximately 2.5mm x 2.5mm were placed on the midline, 60mm from the CWE. The average of the standard deviations of the pixel values in each of the ROIs for each image were used to investigate the relationship between the air kerma incident to the detector and the image noise. A power fit of standard deviation against incident air kerma was made. If electronic and structure noise are small then a square root relationship is expected. It was assumed that the noise in the image comprises three components: electronic noise, structural noise, and quantum noise. The relationship between them is shown in Equation 3:

$$\sigma_p = \sqrt{k_e^2 + k_q^2 p + k_s^2 p^2} \tag{3}$$

where σ_p is the standard deviation in pixel values within an ROI with a uniform exposure and a mean pixel value p, and k_e, k_q, and k_s are the coefficients determining the amount of electronic, quantum, and structural noise in a pixel with a value p. This method of

analysis has been described previously.[8] For simplicity, the noise is generally presented here as relative noise defined as in Equation 4.

$$\text{Relative noise} = \frac{\sigma_p}{p} \tag{4}$$

The variation in relative noise with mean pixel value was evaluated and fitted using Equation 3, and non-linear regression used to determine the best fit for the constants and their asymptotic confidence limits (using Graphpad Prism version 7.00 for Windows, Graphpad software, San Diego, California, USA, www.graphpad.com). This established whether the experimental measurements of the noise fitted this equation, and the relative proportions of the different noise components. The relationship between noise and pixel values has been found empirically to be approximated by a simple power relationship as shown in Equation 5.

$$\frac{\sigma_p}{p} = k_t\, p^{-n} \tag{5}$$

where k_t is a constant. If the noise were purely quantum noise the value of n would be 0.5. However the presence of electronic and structural noise means that n can be slightly higher or lower than 0.5. For graphical presentation in this report pixel values were converted to incident air kerma at the detector using the detector response data described in section 2.3.

The variance in pixel values within a ROI is defined as the standard deviation squared. The total variance against incident air kerma at the detector was fitted using Equation 3. Non-linear regression was used to determine the best fit for the constants and their asymptotic confidence limits, using the Graphpad Prism software.

Using the calculated constants, the structural, electronic, and quantum components of the variance were estimated, assuming that each component was independently related to incident air kerma. The percentage of the total variance represented by each component was then calculated and plotted against incident air kerma at the detector.

2.8   Image quality measurements

Contrast detail measurements were made using a CDMAM phantom (serial number 1022, version 3.4, UMC St. Radboud, Nijmegen University, Netherlands). The phantom was positioned with a 20mm thickness of PMMA above and below, to give a total attenuation approximately equivalent to 50mm of PMMA or 60mm thickness of typical breast tissue. The exposure factors were chosen to match as closely as possible those selected by the AEC, at the standard dose setting, when imaging a 50mm thickness of PMMA. This procedure was repeated to obtain a representative sample of 16 images at this dose level. Further sets of 16 images of the test phantom were then obtained at other dose levels by manually selecting higher and lower mAs values with the same beam quality.

12

The CDMAM images were read and analysed automatically using Version 1.6 of CDCOM.[9,10] and Version 2.1.0 of CDMAM Analysis (www.nccpm.org). The threshold gold thickness for a typical human observer was predicted using Equation 6.

$$TC_{predicted} = rTC_{auto} \tag{6}$$

where $TC_{predicted}$ is the predicted threshold contrast for a typical observer, TC_{auto} is the threshold contrast measured using an automated procedure with CDMAM images. r is the average ratio between human and automatic threshold contrast determined experimentally with the values shown in Table 4.

The contrasts used in Equation 6 were calculated from gold thickness using the effective attenuation coefficient shown in Table 2.

Table 4. Values of r used to predict threshold contrast

Diameter of gold disc (mm)	Average ratio of human to automatically measured threshold contrast (r)
0.08	1.40
0.10	1.50
0.13	1.60
0.16	1.68
0.20	1.75
0.25	1.82
0.31	1.88
0.40	1.94
0.50	1.98
0.63	2.01
0.80	2.06
1.00	2.11

The predicted threshold gold thickness for each detail diameter in the range 0.1mm to 1.0mm was fitted with a curve for each dose level, using the relationship shown in Equation 7.

$$\text{Threshold gold thickness} = a + bx^{-1} + cx^{-2} + dx^{-3} \tag{7}$$

where x is the detail diameter, and a, b, c and d are coefficients adjusted to obtain a least squares fit.

The confidence limits for the predicted threshold gold thicknesses have been previously determined by a sampling method using a large set of images. The threshold contrasts

13

quoted in the tables of results are derived from the fitted curves, as this has been found to improve accuracy.

The expected relationship between threshold contrast and MGD is shown in Equation 8.

Threshold contrast$=\lambda D^{-n}$ (8)

where D is the MGD for a 60mm thick standard breast (equivalent to the test phantom configuration used for the image quality measurement), and λ is a constant to be fitted.

It is assumed that a similar equation applies when using threshold gold thickness instead of contrast. This equation was plotted with the experimental data for detail diameters of 0.1 and 0.25mm. The value of n resulting in the best fit to the experimental data was determined, and the doses required for target CNR values were calculated for data relating to these detail diameters.

The MGDs to reach the minimum and achievable image quality standards in the NHSBSP protocol were then estimated. The error in estimating these doses depends on the accuracy of the curve fitting procedure, and pooled data for several systems has been used to estimate 95% confidence limits of about 20%.

2.9 Physical measurements of the detector performance

The modulation transfer function (MTF), normalised noise power spectrum (NNPS) and the detective quantum efficiency (DQE) of the system were measured. The methods used were as close as possible to those described by the International Electrotechnical Commission (IEC).[11] The radiation quality used for the measurements was adjusted by placing a uniform 2mm thick aluminium filter at the tube housing. The beam quality used was 29kV W/Rh. The test device to measure the MTF comprised a 100mm x 80mm rectangle of stainless steel with a polished straight edge, of thickness 2mm. This test device was placed directly on the breast support table, and the grid was removed. The test device was positioned to measure the MTF in two directions, first almost perpendicular to the CWE and then almost parallel to it. A 10th order polynomial fit was applied to the results.

To measure the noise power spectrum the test device was removed and exposures made for a range of incident air kerma at the surface of the table. The DQE is presented as the average of measurements in the directions perpendicular and parallel to the CWE.

2.10 Other tests

Other tests were carried out to cover the range that would normally form part of a commissioning survey on new equipment. These included tests prescribed in IPEM

Report 89[4] for mammographic X-ray sets, as well as those in the UK NHSBSP protocol for digital mammographic systems.

3. Results

3.1 Output and HVL

The output and HVL measurements are shown in Table 5.

Table 5. Output and HVL

kV	Target/ filter	Output (μGy/mAs at 1m)	HVL (mm Al)
25	W/Rh	8.2	0.50
28	W/Rh	11.4	0.53
31	W/Rh	14.5	0.55
34	W/Rh	17.6	0.57
37	W/Rh	20.7	0.59

3.2 Detector response
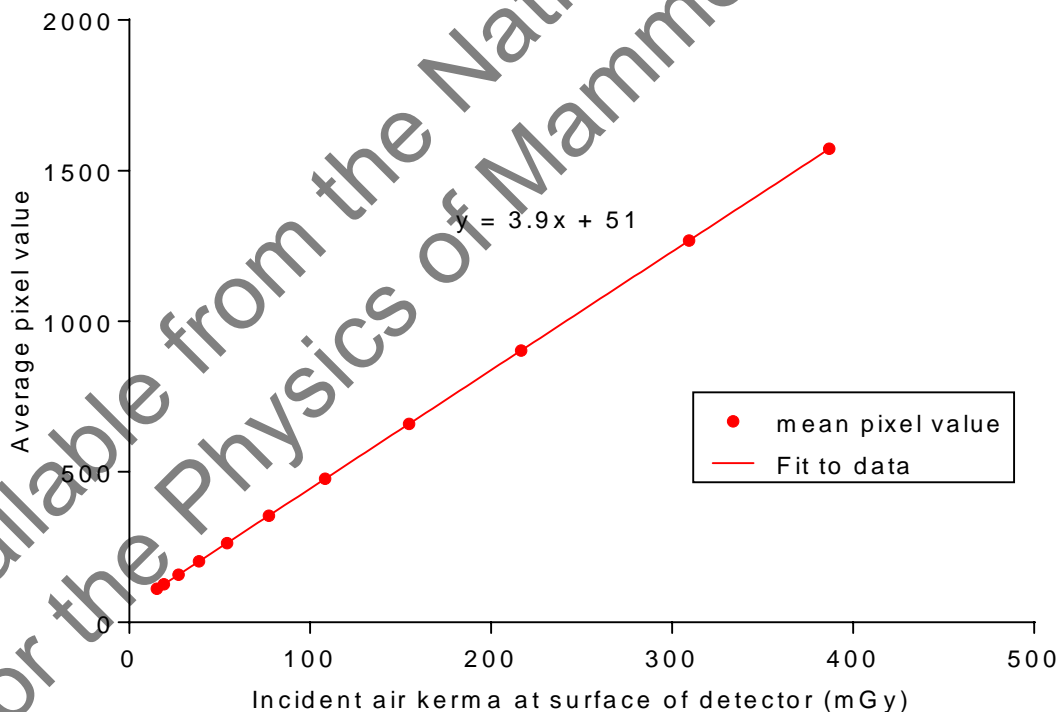
The detector response is shown in Figure 4.

Figure 4. Detector response acquired at 29kV W/Rh anode/filter combination with 2mm Al at the tube port

3.3   AEC performance

3.3.1 Dose

The MGDs for breasts simulated with PMMA exposed under AEC control are shown in Tables 6 and 7 for exposures made in grid mode and with PRIME respectively. These results were acquired with segmentation off, which is appropriate for physics measurements of uniform blocks. The mAs values exclude the pre-exposure. The MGDs were calculated from the total mAs, including the pre-exposure.

Table 6. MGD for simulated breasts (normal dose, grid in, segmentation off)

PMMA thick-ness (mm)	Equivalent breast thickness (mm)	kV	Target/ filter	mAs	MGD (mGy)	Remedial dose level (mGy)	Displ-ayed dose (mGy)	Displayed % higher than measured
20	21	26	W/Rh	30.6	0.44	1.0	0.46	5.3
30	32	27	W/Rh	44.9	0.56	1.5	0.59	6.3
40	45	28	W/Rh	67.1	0.75	2.0	0.78	3.9
45	53	29	W/Rh	75.9	0.86	2.5	0.86	0.0
50	60	30	W/Rh	86.7	0.99	3.0	0.97	-2.3
60	75	31	W/Rh	122.7	1.34	4.5	1.25	-6.8
70	90	32	W/Rh	167.4	1.73	6.5	1.62	-6.3
80	103	32	W/Rh	266.8	2.44	-	2.32	-5.1

Table 7. MGD for simulated breasts (normal dose, PRIME, segmentation off)

PMMA thick-ness (mm)	Equivalent breast thickness (mm)	kV	Target/ filter	mAs	MGD (mGy)	Remedial dose level (mGy)	Displ-ayed dose (mGy)	Displayed % higher than MGD
20	21	26	W/Rh	25.3	0.37	1.0	0.38	2.2
30	32	27	W/Rh	38.1	0.48	1.5	0.50	4.3
40	45	28	W/Rh	59.8	0.67	2.0	0.69	2.3
45	53	29	W/Rh	71.1	0.81	2.5	0.80	-1.1
50	60	30	W/Rh	84.2	0.97	3.0	0.94	-2.7

Note: PRIME only operates for breast thicknesses up to 70mm.

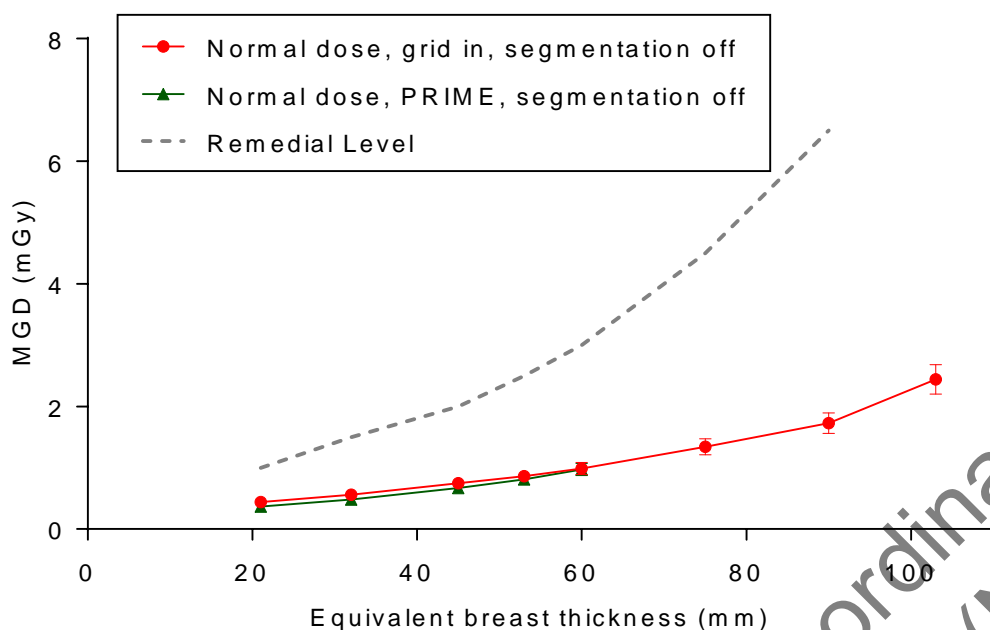The results presented in tables 6 and 7 are also presented graphically in Figure 5.

Figure 5. MGD for different thicknesses of simulated breasts using AEC normal dose mode. (Error bars indicate 95% confidence limits.)

Results of the measurements at different AEC settings are shown in Table 8. The differences in the measured doses were close to the nominal values expected.

Table 8. MGD for simulated breasts at different doses (grid in, segmentation off)

AEC Setting	PMMA Thickness (mm)	kV	Target/ filter	mAs	MGD (mGy)	% of normal dose	Nominal % of normal dose
Low	45	29	W/Rh	62.0	0.71	83	80
Medium Low	45	29	W/Rh	68.3	0.78	90	90
Normal	45	29	W/Rh	76.1	0.86	100	100
Medium High	45	29	W/Rh	85.3	0.96	111	110
High	45	29	W/Rh	93.1	1.04	121	120

18

3.3.2 Contrast-to-Noise ratio

The results of the CNR measurements for images acquired in grid mode and with PRIME are shown in Tables 9 and 10 respectively and in Figure 6. The following calculated values are also shown:

- CNR to meet the minimum acceptable image quality standard
- CNR to meet the achievable image quality standard
- CNRs at each thickness to meet the limiting value in the European protocol

Table 9. CNR measurements (normal dose, grid in, segmentation off)

PMMA (mm)	Equivalent breast thickness (mm)	Measured CNR	CNR for minimum acceptable IQ	CNR for achievable IQ	European limiting CNR value
20	21	10.0	4.5	6.6	5.1
30	32	9.2	4.5	6.6	4.9
40	45	8.5	4.5	6.6	4.7
45	53	8.1	4.5	6.6	4.6
50	60	7.3	4.5	6.6	4.5
60	75	6.5	4.5	6.6	4.2
70	90	5.6	4.5	6.6	4.0
80	103	5.2	4.5	6.6	4.0

Table 10. CNR measurements (normal dose, PRIME, Segmentation off)

PMMA (mm)	Equivalent breast thickness (mm)	Measured CNR	CNR for minimum acceptable IQ	CNR for achievable IQ	European limiting CNR value
20	21	9.4	4.5	6.6	5.1
30	32	8.4	4.5	6.6	4.9
40	45	7.8	4.5	6.6	4.7
45	53	7.5	4.5	6.6	4.6
50	60	6.6	4.5	6.6	4.5

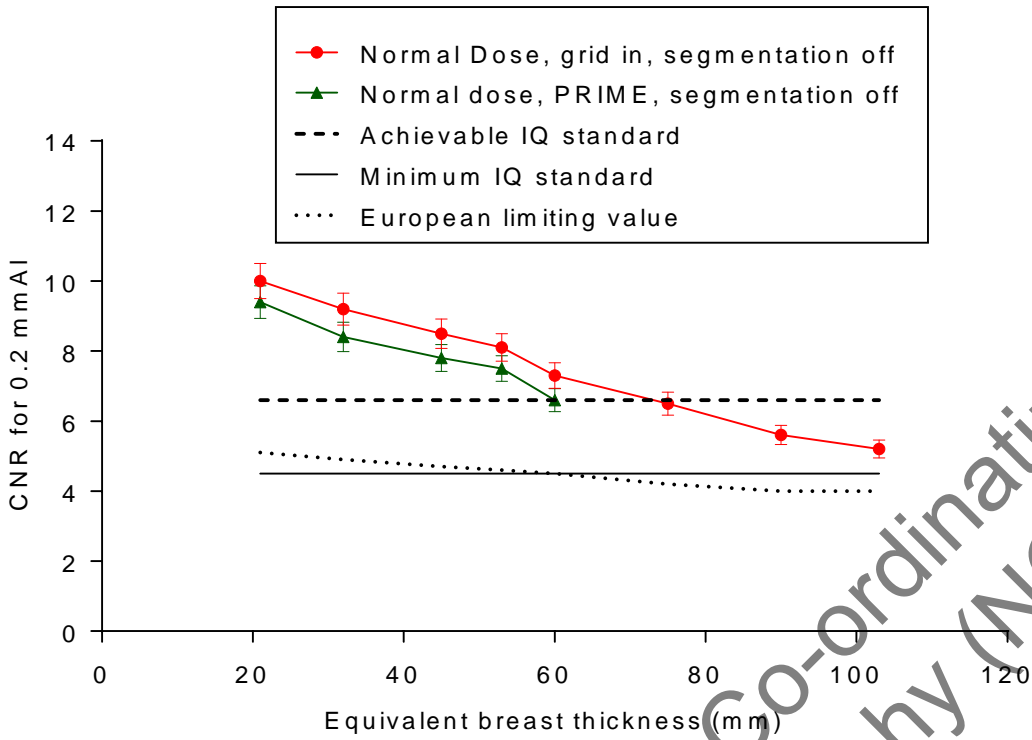Note: PRIME only operates for breast thicknesses up to 70mm.

Figure 6. Measured CNR compared with the limiting values in the European protocol. (Error bars indicate 95% confidence limits.)

3.3.3 AEC performance for local dense areas

In grid mode (without PRIME) and with segmentation on, it is expected that when the AEC adjusts for local dense areas, the SNR remains constant with increasing thickness of extra PMMA. The results presented in Table 11 and Figure 7 show that the SNR does remain constant as thickness increases up to a total attenuation of 40mm PMMA. Above 40mm PMMA the mAs values selected by the AEC falls and a corresponding drop in the SNR was seen.

20

Table 11. AEC performance for local dense areas

Total attenuation (mm PMMA)	kV	Target / filter	Tube load (mAs)	SNR	% SNR difference from mean SNR result
30	28	W/Rh	66.3	85.3	16
32	28	W/Rh	66.6	80.0	9
34	28	W/Rh	70.3	81.2	11
36	28	W/Rh	77.2	80.8	10
38	28	W/Rh	84.5	81.1	11
40	28	W/Rh	91.9	75.7	3
42	28	W/Rh	66.7	65.1	11
44	28	W/Rh	66.6	64.3	12
46	28	W/Rh	66.7	59.4	19
48	28	W/Rh	66.7	60.4	19
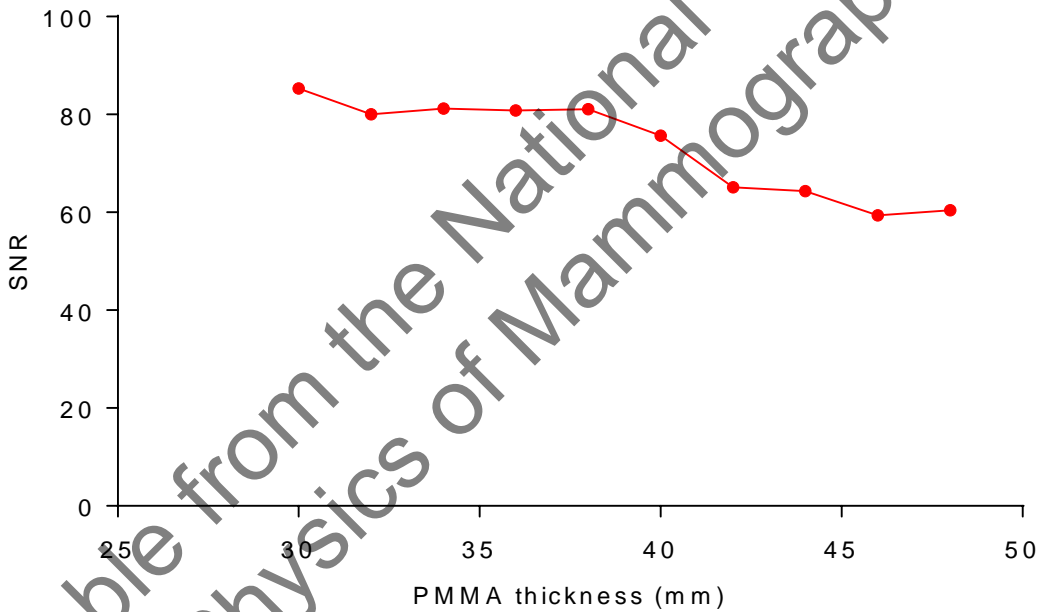
Figure 7. AEC performance for local dense areas

3.4 Noise measurements

The variation in noise with dose was analysed by plotting the standard deviation in pixel values against the incident air kerma to the detector, as shown in Figure 8. The fitted

power curve has an index of 0.50, which is the expected value for quantum noise sources alone.
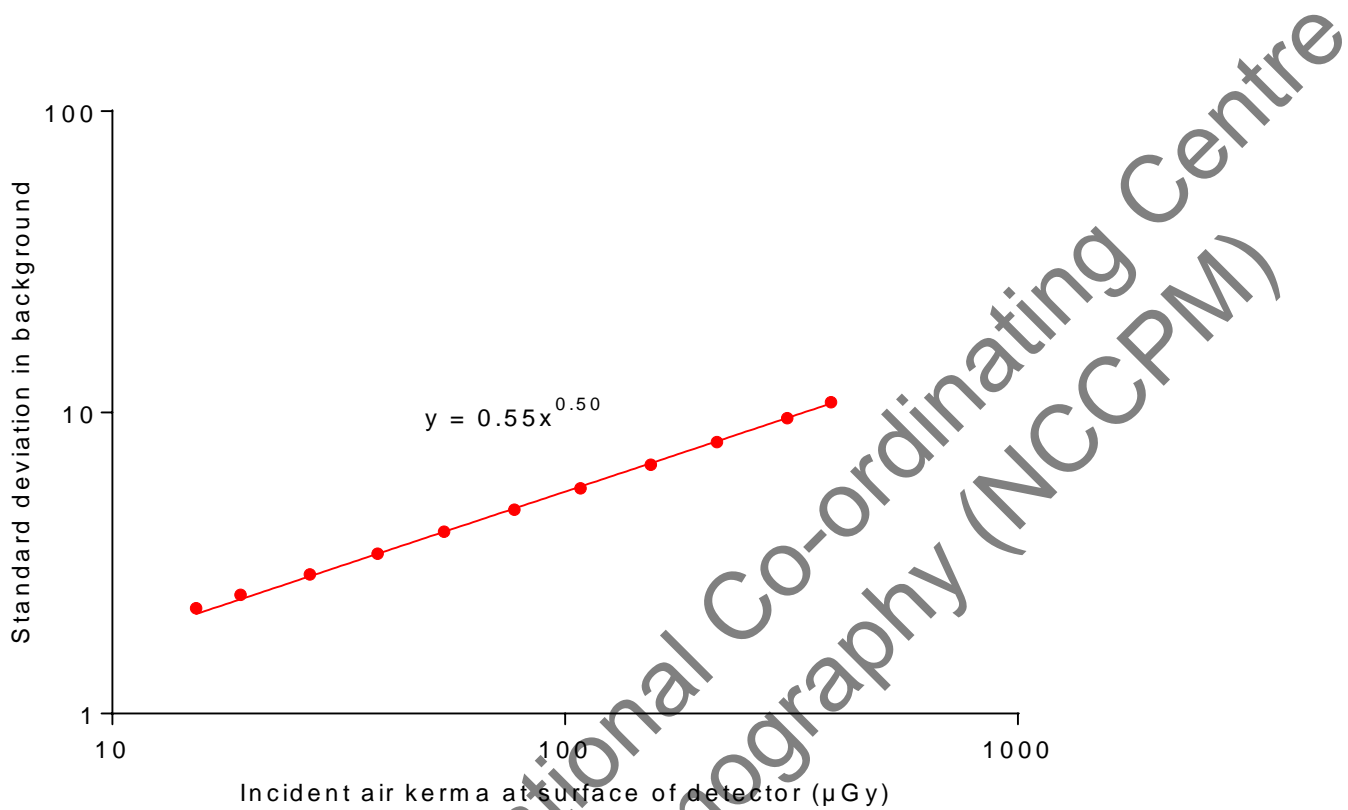

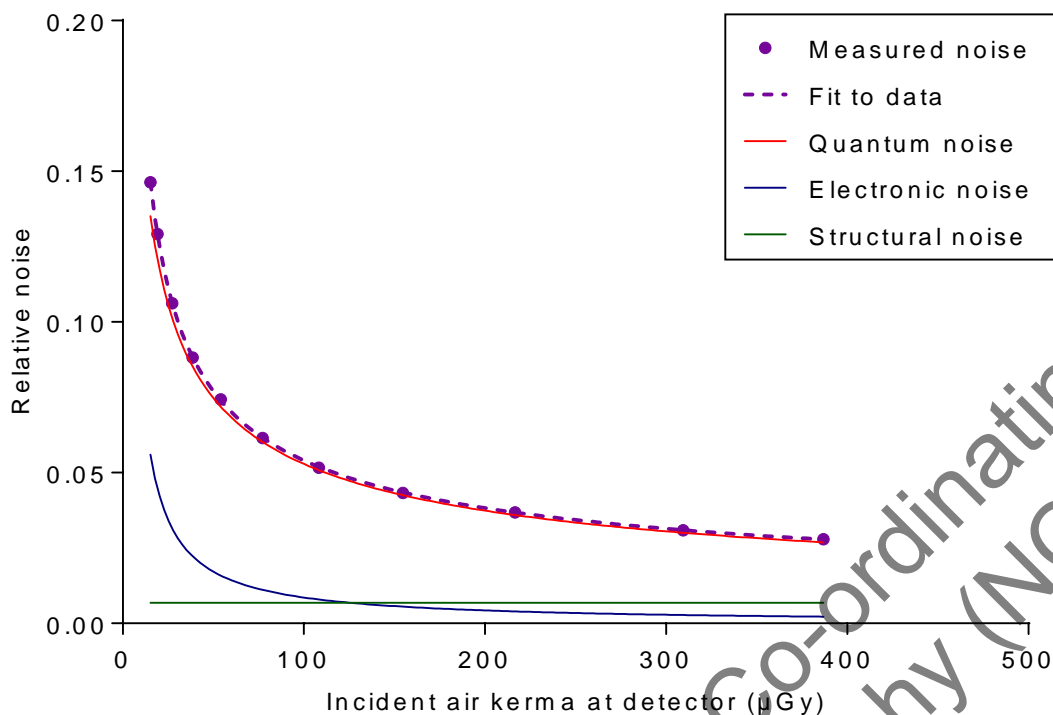**Figure 8. Standard deviation of linearized pixel values versus incident air kerma at detector**

Figure 9. Relative noise and noise components

Figure 9 shows the relative noise at different incident air kerma. The estimated relative contributions of electronic, structural, and quantum noise are shown and the quadratic sum of these contributions fitted to the measured noise (using Equation 3).

Figure 10 shows the different amounts of variance due to each component. From this, the dose range over which the quantum component dominates can be seen.
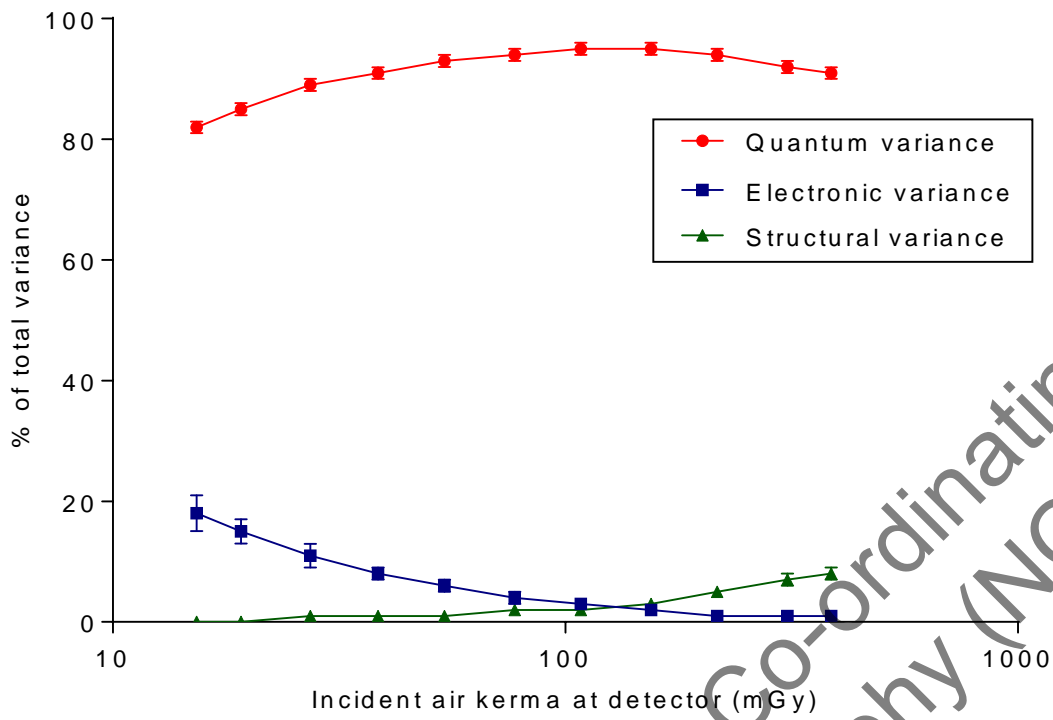
Figure 10. Noise components as a percentage of the total variance (Error bars indicate 95% confidence limits.)

3.5   Image quality measurements

The exposure factors used for each set of 16 CDMAM images are shown in Table 12. The MGDs ranged from half to three times the dose of 0.87mGy, which was close to that selected for the equivalent breast of 60mm thick in AEC mode.

Table 12. Images acquired for image quality measurement

kV	Target/filter	Tube loading (mAs)	Mean glandular dose to equivalent breasts 60mm thick (mGy)
30	W/Rh	36	0.39
30	W/Rh	50	0.54
30	W/Rh	80	0.87
30	W/Rh	110	1.19
30	W/Rh	180	1.95
30	W/Rh	250	2.71

The contrast detail curves (determined by automatic reading of the images) at the different dose levels are shown in Figure 11. The threshold gold thicknesses measured for different detail diameters at the 6 selected dose levels are shown in Table 13. The NHSBSP minimum acceptable and achievable limits are also shown.
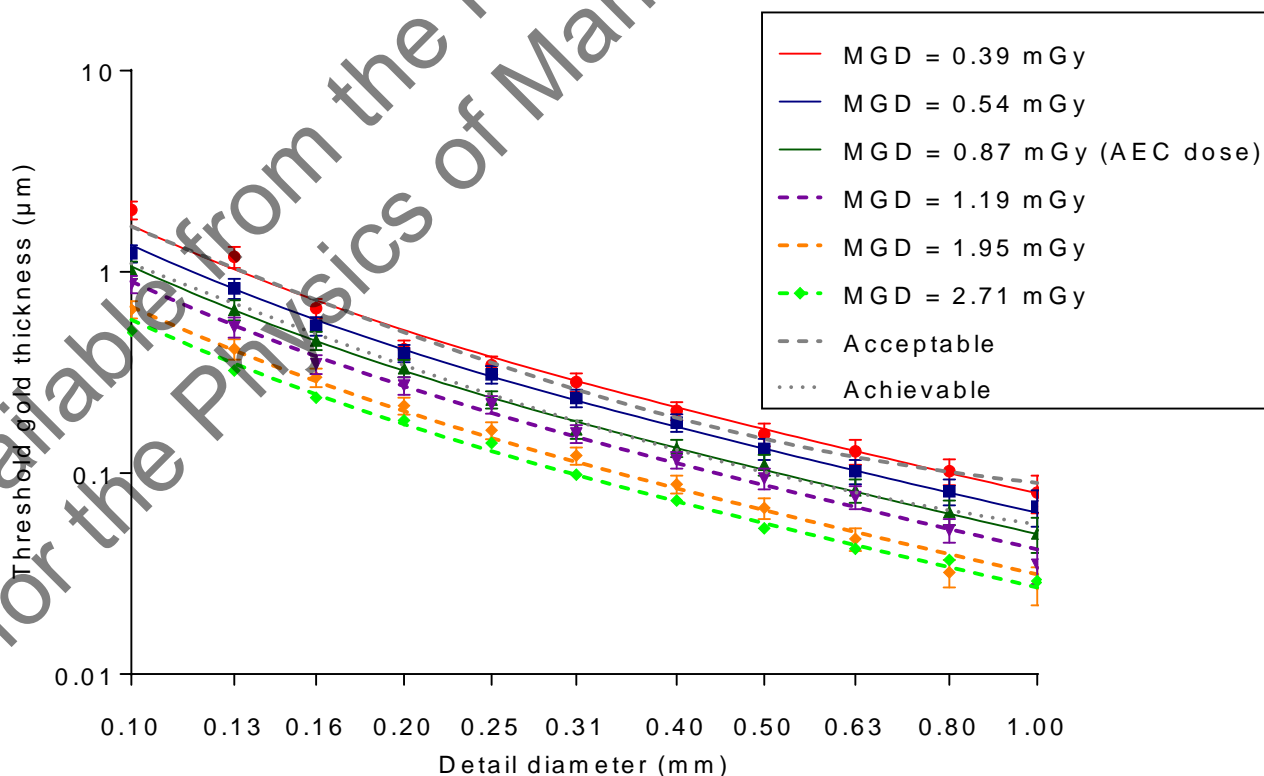
Figure 11. Threshold gold thickness detection curves for 6 doses at 30kV W/Rh. (Error bars indicate 95% confidence limits.)

Table 13. Average threshold gold thicknesses for different detail diameters for 6 doses using 30kV W/Rh, and automatically predicted data

Diameter (mm)	Acceptable value	Achievable value	Threshold gold thickness (µm)					
			Mean Glandular Dose to equivalent breast 60mm thick (mGy)					
			0.39	0.54	0.87	1.19	1.95	2.71
0.1	1.680	1.100	2.03 ± 0.21	1.24 ± 0.12	1.02 ± 0.10	0.87 ± 0.09	0.65 ± 0.06	0.51 ± 0.05
0.25	0.352	0.244	0.34 ± 0.04	0.31 ± 0.03	0.33 ± 0.03	0.22 ± 0.02	0.16 ± 0.02	0.14 ± 0.01
0.5	0.150	0.103	0.16 ± 0.02	0.13 ± 0.02	0.11 ± 0.01	0.09 ± 0.01	0.07 ± 0.01	0.05 ± 0.01
1	0.091	0.056	0.08 ± 0.02	0.07 ± 0.01	0.05 ± 0.01	0.04 ± 0.01	0.03 ± 0.01	0.03 ± 0.01

The measured threshold gold thicknesses are plotted against the MGD for an equivalent breast for the 0.1mm and 0.25mm detail sizes in Figure 12.
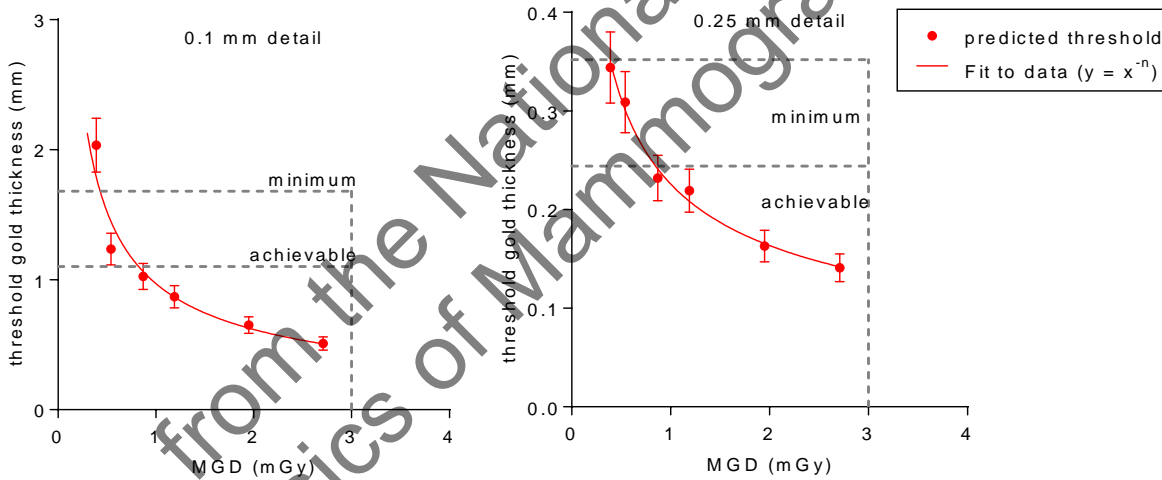

Figure 12. Threshold gold thickness at different doses. (Error bars indicate 95% confidence limits.)

3.6 Comparison with other systems

The MGDs to reach the minimum and achievable image quality standards in the NHSBSP protocol have been estimated from the curves shown in Figure 13. These doses are shown against similar data for different models of digital mammography systems in Tables 14 and 15 and Figures 13 to 16. The data for these systems has been determined in the same way as described in this report and the results published

previously.[12-18] The data for film-screen represents an average value determined using a variety of film-screen systems in use prior to their discontinuation.

Table 14. The MGD for a 60mm equivalent breast for different systems to reach the minimum threshold gold thickness for 0.1mm and 0.25mm details

System	MGD (mGy) for 0.1mm	MGD (mGy) for 0.25mm
Fujifilm Innovality	0.61 ± 0.12	0.49 ± 0.10
GE Essential	0.49 ± 0.10	0.49 ± 0.10
Hologic Dimensions (v1.4.2)	0.34 ± 0.07	0.48 ± 0.10
Hologic Selenia (W)	0.71 ± 0.14	0.64 ± 0.13
IMS Giotto 3DL	0.93 ± 0.19	0.70 ± 0.14
Philips MicroDose L30 C120	0.67 ± 0.13	0.47 ± 0.09
Planmed Clarity 2D	0.60 ± 0.12	0.49 ±0.10
Siemens Inspiration	0.76 ± 0.15	0.60 ± 0.12
Siemens Revelation	**0.43 ± 0.09**	**0.39 ± 0.08**
Film-screen	1.30 ± 0.26	1.36 ± 0.27

Table 15. The MGD for a 60mm equivalent breast for different systems to reach the achievable threshold gold thickness for 0.1mm and 0.25mm details

| System	MGD (mGy) for 0.1mm	MGD (mGy) for 0.25mm
Fujifilm Innovality	1.15 ± 0.23	1.02 ± 0.20
GE Essential	1.13 ± 0.13	1.03 ± 0.21
Hologic Dimensions (v1.4.2)	0.87 ± 0.17	1.10 ± 0.22
Hologic Selenia (W)	1.37 ± 0.27	1.48 ± 0.30
IMS Giotto 3DL	1.60 ± 0.32	1.41 ± 0.28
Philips MicroDose L30 C120	1.34 ± 0.27	1.06 ± 0.21
Planmed Clarity 2D	1.15 ± 0.23	1.02 ± 0.20
Siemens Inspiration	1.27 ± 0.25	1.16 ± 0.23
Siemens Revelation	**0.82 ± 0.17**	**0.85 ± 0.17**
Film-screen	3.03 ± 0.61	2.83 ± 0.57
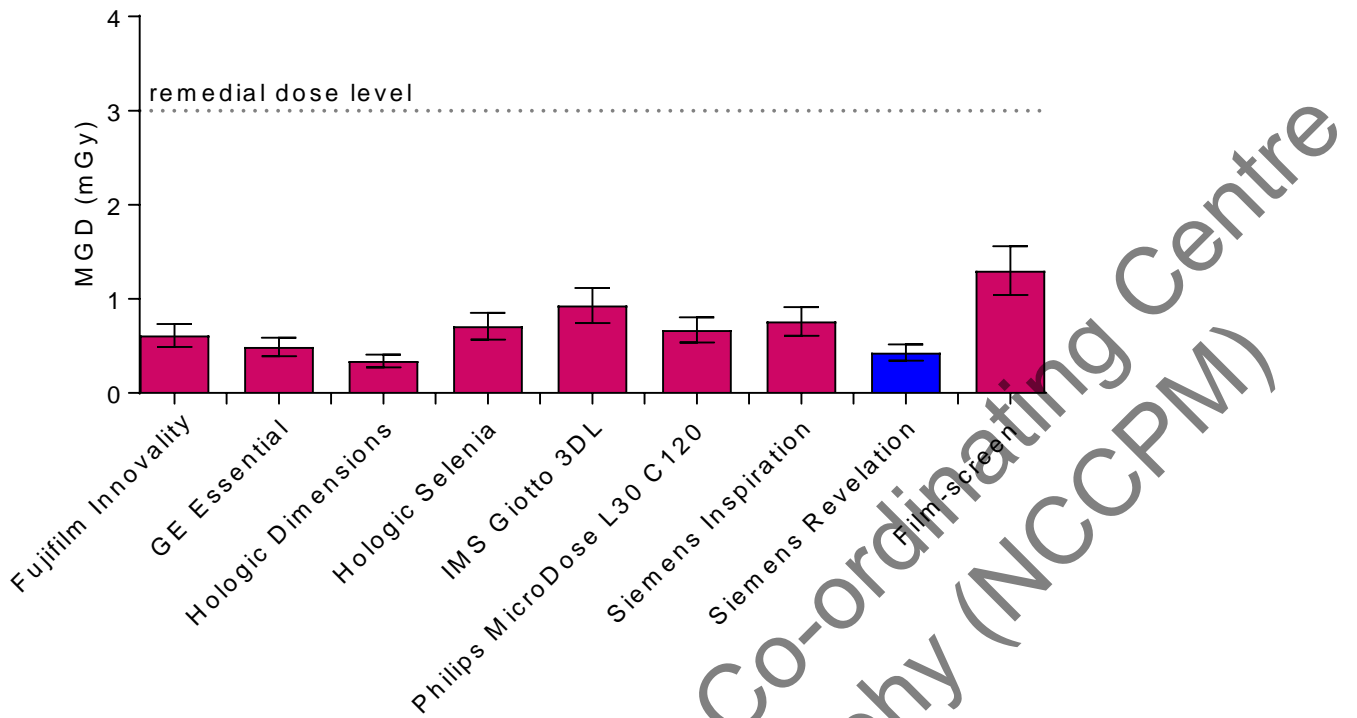
Figure 13. MGD for a 60mm equivalent breast to reach minimum acceptable image quality standard for 0.1mm detail. (Error bars indicate 95% confidence limits.)
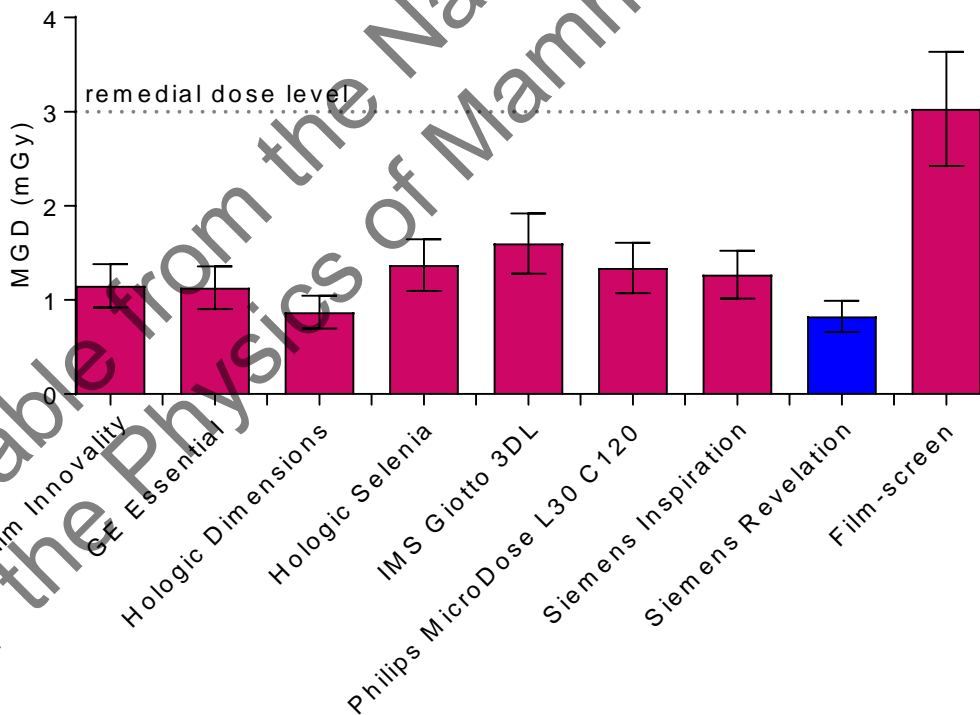

Figure 14. MGD for a 60mm equivalent breast to reach achievable image quality standard for 0.1mm detail. (Error bars indicate 95% confidence limits.)
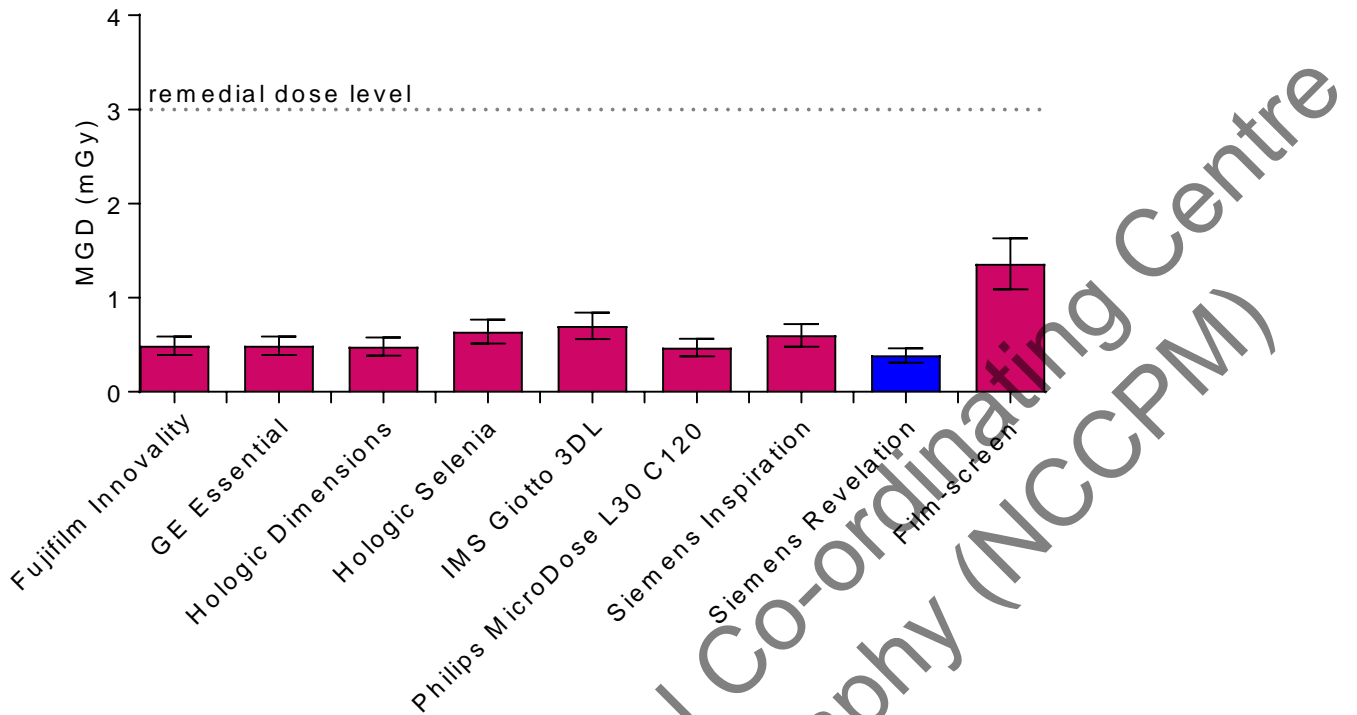
Figure 15. MGD for a 60mm equivalent breast to reach minimum acceptable image quality standard for 0.25mm detail. (Error bars indicate 95% confidence limits.)
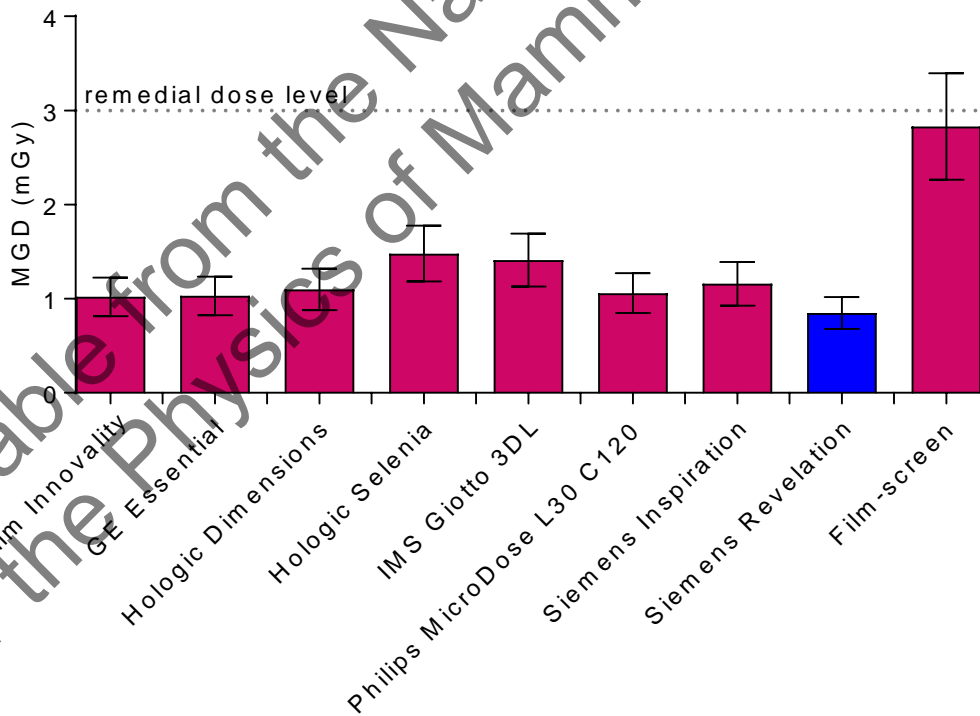

Figure 16. MGD for a 60mm equivalent breast to reach achievable image quality standard for 0.25mm detail. (Error bars indicate 95% confidence limits.)

3.7   Detector performance

The MTF is shown in Figure 17 for the two orthogonal directions. Figure 18 shows the NNPS curves for a range of air kerma incident to the detector.
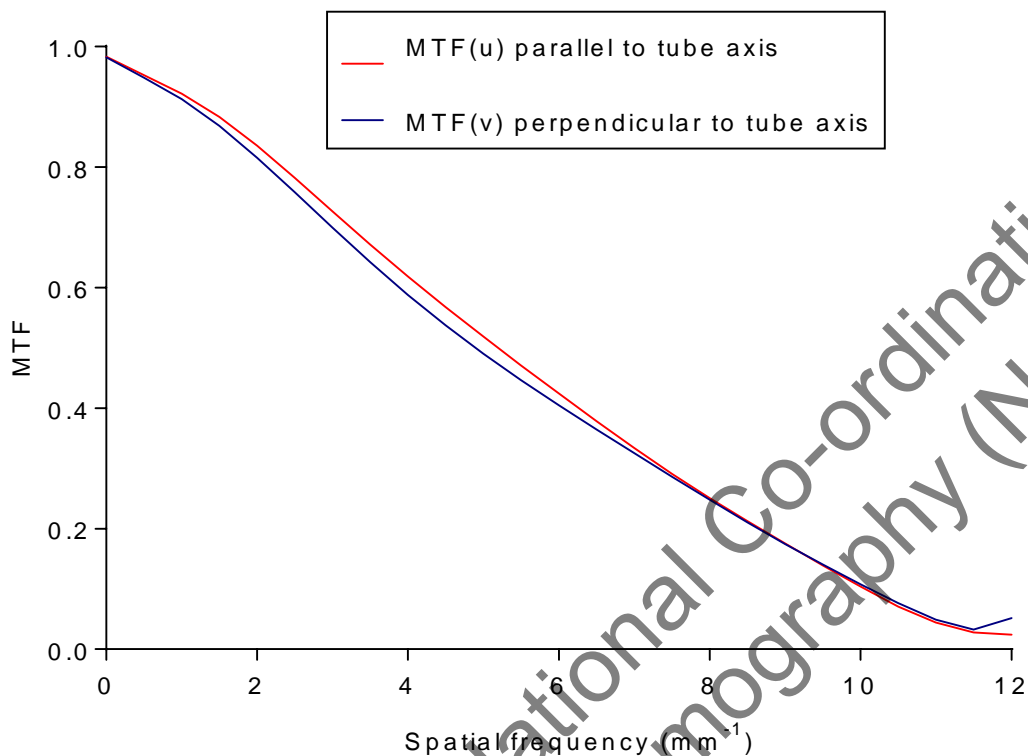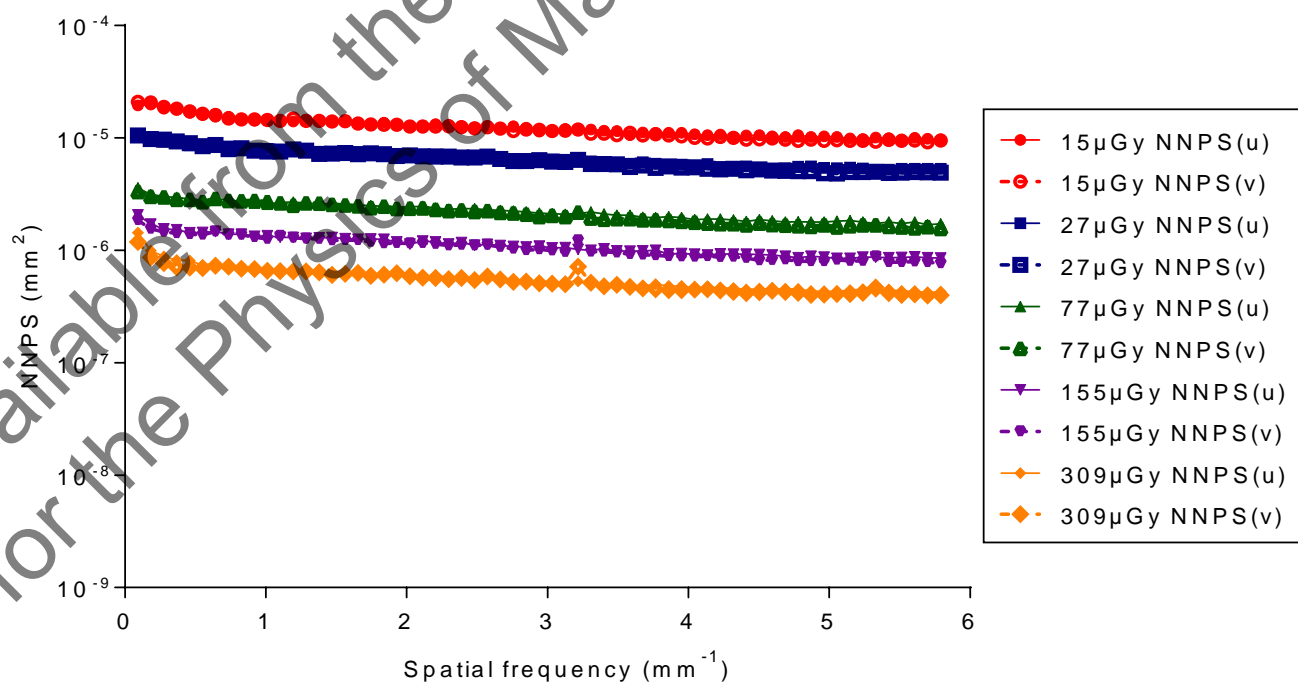

Figure 17. Pre-sampled MTF

Figure 18. NNPS curves for a range of air kerma incident to the detector

31

Figure 19 shows the DQE averaged in the two orthogonal directions for a range of incident air kerma. The MTF and DQE measurements were interpolated to show values at standard frequencies in Table 16.
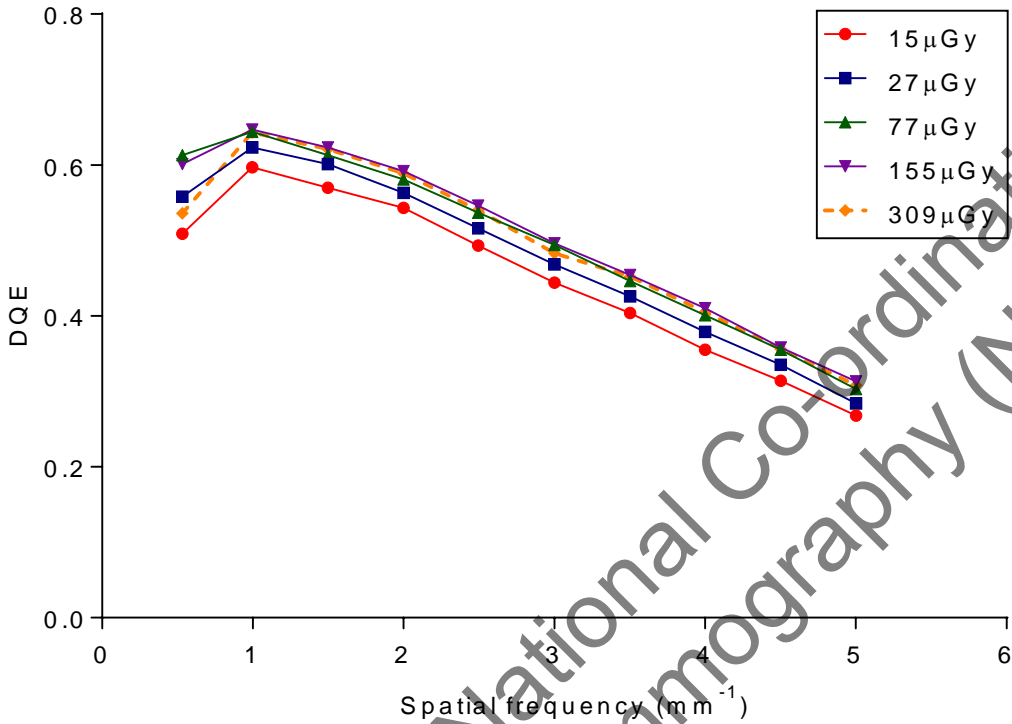
Figure 19. DQE averaged in both directions for a range of incident air kerma

Table 16. MTF and DQE measurements at standard frequencies (DQE at incident air kerma of 77µGy)

Frequency (mm⁻¹)	MTF (u)	MTF (v)	DQE
0.0	1	1	-
0.5	0.95	0.95	0.61
1.0	0.92	0.91	0.64
1.5	0.88	0.87	0.61
2.0	0.84	0.82	0.58
2.5	0.78	0.76	0.54
3.0	0.73	0.70	0.49
3.5	0.67	0.64	0.45
4.0	0.62	0.59	0.40
4.5	0.57	0.54	0.35
5.0	0.52	0.49	0.30

3.8 Detector warm-up

Table 17 shows the CNR measured at intervals after switching the system on.

Table 17. CNR for 2D images acquired after the system was switched on

Time (min)	PMMA thickness (mm)	Equivalent breast thickness (mm)	kV	Target/ filter	mAs	CNR
1	45	53	29	W/Rh	76.1	6.7
6	45	53	29	W/Rh	75.5	6.8
10	45	53	29	W/Rh	76.1	6.8
21.5	45	53	29	W/Rh	76.1	6.9
30	45	53	29	W/Rh	75.3	7.1
40	45	53	29	W/Rh	76.1	7.5
50	45	53	29	W/Rh	76.5	7.5
60	45	53	29	W/Rh	76.1	7.6

Over the period of the test the CNR was seen to increase by 13%.

3.9 Other tests

The results of all the other tests that were carried out were within acceptable limits as prescribed in the UK protocol and IPEM Report 89.[4]

3.9.1 Tube voltage

The tube voltage measurements are shown in Table 18. All were within 0.8kV of indicated values and compared favourably with the IPEM Report 89[4] remedial level of 1kV.

Table 18. Tube voltage measurements

Set voltage (kV)	Measured voltage (kV)
26	26.8
27	27.6
28	28.5
29	29.5
30	30.1
31	30.8
32	31.9

3.9.2 Compression

The measured compressed breast thicknesses are compared with the displayed values in Table 19. They were within 2mm of displayed values. This is well within the IPEM Report 89[4] remedial level of less than or equal to 5mm.

Measurements of compression force together with IPEM89 remedial levels are shown in Table 20.

Table 19. Indicated compressed breast thickness

Actual thickness (mm)	Indicated thickness (mm)	Difference (mm)
20	20	0
40	39	1
60	58	2

Table 20. Compression force

	Measured force (N)	IPEM89 remedial level
Difference between indicated and measured compression	13	>20N
Maximum motorised compression	188	<150N or >200N
Compression change over 30 seconds	3	>20N

3.9.3 Alignment

Alignment measurements for the 200 x 270mm, 240mm x 300mm and 180mm x 240mm (central, left & right shift positions) field sizes showed that the light field edges were all within 4mm of the edges of the radiation field (IPEM remedial level > 5mm) except at the front edge where there was an overlap of up to 7mm. The radiation field overlapped the edges of the image by up to 4mm (remedial level < 0mm or > 5mm).

3.9.4 Image retention

The image retention factor was 0.01, compared to the NHSBSP upper limit of 0.3.

3.9.5 AEC repeatability

For a series of 5 repeat images, acquired in quick succession, the maximum deviation of mAs from the mean was 0.5%. The variation in SNR was less than 1%. For 5 images, acquired at intervals over several days of testing, the maximum deviation in mAs was 4.1%. The NHSBSP remedial level is 5%.

3.9.6 Uniformity and artefacts

Uniformity measurements showed a variation in pixel values of less than 3% relative to the central area. The NHSBSP remedial level is 10%.

3.9.7 Cycle time

For a typical exposure of 45mm PMMA using 29kV W/Rh and 76mAs, a subsequent exposure could be made 20 seconds after the start of the previous one.

3.9.8 Backup timer

When an AEC exposure was attempted with a brass plate blocking the X-ray beam and 80mm of PMMA, the exposure terminated after a short time of less than a second following the pre-exposure. There was no main exposure and no image acquired.

3.9.9 Focal spot

The measured dimensions of the focal spot were 0.37mm x 0.33mm in broad focus and 0.17mm x 0.14mm in fine focus.

3.9.10 Mesh

No discontinuities or blurred regions were seen in the image of the mesh test object.

4. Discussion

4.1 Dose and contrast-to-noise ratio

The detector response was found to be linear. This was as expected for Siemens systems.

MGDs measured using PMMA were well within the NHSBSP remedial dose levels for all equivalent breast thicknesses when using all AEC dose modes. In the normal AEC dose mode the MGD to the 53mm thick standard breast model was 0.86mGy (Table 6).

CNR measurements made with plain PMMA showed an overall decrease in CNR with increased thickness of PMMA (Figure 6). Target CNR values of 4.5 and 6.6, for minimum acceptable and achievable image quality respectively, were calculated from the CNR and threshold gold thickness results.

In the normal dose AEC mode, the CNRs exceeded the target for the achievable level of image quality for equivalent breast thicknesses of up to 60mm. For 75, 90 and 103mm equivalent breast thicknesses, the CNRs were just below the achievable level.

In PRIME mode, MGDs to the standard breast model for equivalent breast thicknesses up to 60mm were 0% to 15% lower than in grid mode. Correspondingly CNRs were measured to be up to 10% lower. It should be noted that these results, measured with uniform blocks, will not necessarily directly relate to the performance of PRIME in clinical use. In clinical use, PRIME mode with segmentation on, works by identifying structures in the breast to both determine the exposure factors and to subtract the calculated scatter. Further information on PRIME and an explanation of how segmentation works is provided in NHSBSP Equipment Report 1503[19].

4.2 Local dense area

The local dense area test showed that with segmentation on the AEC identifies the presence of the dense area and increases the mAs in order to maintain SNR up to a total attenuation of 40mm of PMMA. For a total attenuation greater than 40mm the AEC excludes the dense area and the mAs dropped back to values close to those for 30mm PMMA and a drop in the SNR was seen corresponding to the fall in mAs. Siemens have confirmed that the system is performing as expected.

4.3 Noise analysis

Noise analysis showed that quantum noise dominates the noise over the whole range of incident air kermas that noise was measured (15 to 400µGy) (Figure 10). There are minimal contributions from electronic and structural noise.

4.4   Image quality

Threshold gold thicknesses for a range of detail diameters are shown in Figure 11. At an MGD of 0.87mGy (close to that selected for the equivalent thickness of PMMA in Standard mode), the image quality was better than the achievable level for all contrast detail diameters.

Threshold gold thickness measurements at different dose levels for the 0.1mm and 0.25mm diameter details were used to calculate MGDs to a 60mm equivalent breast required for the minimum and achievable levels of image quality (Figure 12). This allowed comparisons to be made between this and other systems previously tested. The dose required for the Revelation to reach the achievable level of image quality was at the lower end of the range measured for other direct digital mammography systems (Table 15).

4.5   Detector performance

The detector performance, as indicated by MTF, NNPS and DQE curves (Figures 17-19), was provided for reference and was within expected results.

4.6   Other tests

The miscellaneous results presented under the section "Other tests" were satisfactory.

5. Conclusions

The Siemens Revelation in 2D mode meets the minimum requirements of the NHSBSP standards for digital mammography systems when operating in the normal dose AEC mode.

The MGD is well below the remedial level in the normal dose AEC mode. The image quality, as measured by threshold gold thickness, is at the achievable level.

References

1. Kulama E, Burch A, Castellano I et al. *Commissioning and routine testing of full field digital mammography systems* (NHSBSP Equipment Report 0604, Version 3). Sheffield: NHS Cancer Screening Programmes, 2009

2. van Engen R, Young KC, Bosmans H, et al. European protocol for the quality control of the physical and technical aspects of mammography screening. In *European guidelines for quality assurance in breast cancer screening and diagnosis*, Fourth Edition. Luxembourg: European Commission, 2006

3. van Engen R, Bosmans H, Dance D et al. Digital mammography update: European protocol for the quality control of the physical and technical aspects of mammography screening. In *European guidelines for quality assurance in breast cancer screening and diagnosis,* Fourth edition – Supplements. Luxembourg: European Commission, 2013

4. Moore AC, Dance DR, Evans DS et al. *The Commissioning and Routine Testing of Mammographic X-ray Systems.* York: Institute of Physics and Engineering in Medicine, Report 89, 2005

5. Alsager A, Young KC, Oduko JM. Impact of heel effect and ROI size on the determination of contrast-to-noise ratio for digital mammography systems. In *Proceedings of SPIE Medical Imaging*, Bellingham WA: SPIE Publications, 2008, 691341: 1-11

6. Boone JM, Fewell TR and Jennings RJ. Molybdenum, rhodium and tungsten anode spectral models using interpolating polynomials with application to mammography *Medical Physics*, 1997, 24: 1863-1974

7. Berger MJ, Hubbell JH, Seltzer SM, Chang et al. XCOM: Photon Cross Section Database (version 1.3) http://physics.nist.gov/xcom (Gaithersburg, MD, National Institute of Standards and Technology), 2005

8. Young KC, Oduko JM, Bosmans H, Nijs K, Martinez L. Optimal beam quality selection in digital mammography. *British Journal of Radiology*, 2006, 79: 981-990

9. Young KC, Cook JH, Oduko JM. Automated and human determination of threshold contrast for digital mammography systems. In *Proceedings of the 8th International Workshop on Digital Mammography,* Berlin: Springer-Verlag, 2006, 4046: 266-272

10. Young KC, Alsager A, Oduko JM et al. Evaluation of software for reading images of the CDMAM test object to assess digital mammography systems. In *Proceedings of SPIE Medical Imaging*, Bellingham WA: SPIE Publications, 2008, 69131C: 1-11

11.   IEC 62220-1-2, *Determination of the detective quantum efficiency – Detectors used in mammography.* International Electrotechnical Commission, 2007

12.   Young KC, Oduko JM. *Technical evaluation of the Hologic Selenia full field digital mammography system with a tungsten tube* (NHSBSP Equipment Report 0801). Sheffield: NHS Cancer Screening Programmes, 2008

13.   Young KC, Oduko JM, Gundogdu O and Asad M. *Technical evaluation of profile automatic exposure control software on GE Essential FFDM systems* (NHSBSP Equipment Report 0903). Sheffield: NHS Cancer Screening Programmes, 2009

14.   Young KC, Oduko JM, Gundogdu, O, Alsager, A. *Technical evaluation of Siemens Mammomat Inspiration Full Field Digital Mammography System* (NHSBSP Equipment Report 0909). Sheffield: NHS Cancer Screening Programmes, 2009

15.   Young KC, Oduko JM. *Technical evaluation of Hologic Selenia Dimensions 2-D Digital Breast Imaging System with software version 1.4.2* (NHSBSP Equipment Report 1201). Sheffield: NHS Cancer Screening Programmes, 2012

16.   Strudley CJ, Young KC, Oduko JM. *Technical Evaluation of the IMS Giotto 3DL Digital Breast Imaging System* (NHSBSP Equipment Report 1301). Sheffield: NHS Cancer Screening Programmes, 2013

17.   Oduko JM, Young KC. *Technical evaluation of Philips MicroDose L30 with AEC software version 8.3* (NHSBSP Equipment Report 1305). Sheffield: NHS Cancer Screening Programmes, 2013

18.   Strudley CJ, Oduko JM, Young KC. *Technical evaluation of the Fuji AMULET Innovality Digital Breast Imaging System* (NHSBSP Equipment Report 1601). London, Public Health England, 2017

19.   JM Oduko, CJ Strudley, KC Young. *Technical evaluation of the Siemens Inspiration PRIME with VB30L software* (NHSBSP Equipment Report 1503). London, Public Health England, 2016